COBEM 2021 26th International Congress of Mechanical Engineering
November 22-26, 2021, Virtual Congress, Brazil

INVESTIGATION OF DAMPING EFFECTS IN MONOCOUPLED PHONONIC CRYSTALS AND METAMATERIALS

Emanuel Victor Borges de Morais Cruvinel
Romes Antônio Borges
Federal University of Catalão - Mathematics and Technology Institute
emanuelcruvinel@discente.ufg.br
romes@ufg.br

Domingos Alves Rade
Aeronautics Institute of Technology, Division of Mechanical Engineering, Brazil
rade@ita.br

Abstract. *Periodic structures are composed of identical substructures or cells that are connected end to end, with their periodicity characterized by geometrical or material discontinuity. Due to the periodicity, these structures present special dynamic characteristics, acting as mechanical filters for elastic waves propagating in specific frequency intervals, known as stop bands or band gaps. The large majority of previous investigations disregard energy dissipation effects. However, real structures dissipate energy by various mechanisms, for instance, due to friction at connections, opening and closing of microcracks or internal friction. Energy dissipation, also characterized as vibration damping, can alter frequency band structures, thus modifying the behavior of wave propagation. The purpose of this paper is to analyze the effect of damping on elastic waves attenuation of periodic structures when subjected to forced harmonic excitation. The viscous model damping applied to four different configurations of periodic structures, with and without internal resonators, modeled as lumped mass-spring-damper subsystems is investigated. For each configuration, the equations of motion of the unit cell are derived, and the transfer matrix method is implemented to model the elastic wave propagation along the periodic structure and to obtain the propagation constant that allows the construction of dispersion curves. Different levels of damping are considered, and their effects in pass bands, stop bands and frequency response functions are analyzed.*

Keywords: *periodic structures, stop bands, band gaps, damping, acoustic metamaterials*

1. INTRODUCTION

Periodic structures emerge in a variety of engineering applications, ranging from aircrafts fuselage and bridges to satellite panels and railway tracks. The periodicity arises from repeated geometrical or material pattern along the dimensions of the structure, and can induce an interesting phenomenon called elastic *bandgaps* (Hussein *et al.*, 2014). These are frequency ranges where elastic waves do not propagate, in a similar fashion to electromagnetic waves in electrical insulators. This mechanism is related to the elastic wave interference throughout the structure periodic boundaries where destructive interference takes place as a consequence of different travelling wave speeds in each medium.

Most of the investigations presented in the literature regarding periodic structures ignores energy dissipation. Since real structures dissipate some amount of vibrational energy when subjected to free or forced vibration (Beards, 1996), the characteristics of waves propagation through structures is altered, thus influencing the position and breadth of pass bands and bandgaps (Hussein and Frazier, 2010). Hence, it is necessary to account for damping effects in the equations of motion of periodic structures in order to obtain its real dynamics.

Two common frameworks are used when analyzing bandgaps from the so-called dispersion diagrams (maps wavenumber vs frequency) namely, the free wave and the prescribed wave propagation (Krattiger *et al.*, 2017). The former deals with responses to initial conditions whereas the latter considers forced harmonic responses. Using the free wave propagation, the wavenumber input is selected to be a real number, and the frequency solutions are permitted to be complex. On the other hand, the prescribed wave propagation allows the frequency input to be real, and thus the wavenumber solutions are complex. Since the investigation in this paper is related to harmonic excitation sources applied in periodic structures, the prescribed wave propagation framework is utilized.

The present paper deals with damping in periodic structures, particularly in monocoupled phononic crystals and metamaterials. Considering four different configurations, the equations of motion for each unit cell are derived, and dissipation is modeled using a proportional viscous damping model. The transfer matrix method is employed for the

construction of dispersion diagrams where the location of pass bands and bandgaps are observed. Moreover, the frequency response function (FRF) of each periodic structure with a finite number of unit cells is also plotted, allowing the inspection of admittance levels when damping is introduced.

This paper is structured as follows: the transfer matrix method is reviewed in Section 2. The equation of motion for a diatomic mass spring is developed, and the steps to obtain the propagation constant to plot the band gaps and stop bands are listed. Next, in Section 3, a brief discussion of each damped periodic structure is carried out. Finally, in section 4, numerical experiments are done in four different configurations of damped periodic structures, where the first two cases encompass phononic crystals and the last two are metamaterials featuring internal resonators. The proportional viscous damping model is applied to the unit cell of each case, with a prescribed damping ratio set to the first vibrational mode. The effect of damping is then analyzed in the pass and stop bands of the dispersion diagram, as well as in the FRFs and spatial attenuation of the structures.

2. TRANSFER MATRIX METHOD

In order to obtain the dispersion diagrams of the periodic structures, the transfer matrix method is illustrated in this section. For this, consider the general equation of motion represented in Eq. (1):

$$\mathbf{M}\ddot{\mathbf{q}} + \mathbf{C}\dot{\mathbf{q}} + \mathbf{K}\mathbf{q} = \mathbf{F}. \tag{1}$$

For the implementation of the transfer matrix method, it is useful to place Eq. (1) in the frequency domain:

$$(\mathbf{K} + j\omega\mathbf{C} - \omega^2\mathbf{M})\mathrm{q} = \mathbf{F}. \tag{2}$$

The term inside parenthesis is called the dynamic stiffness matrix, and it is represented by the matrix $D(\omega)$. Thus, Eq. (2) is rewritten as:

$$\mathbf{D}(\omega)\mathbf{q} = \mathbf{F}. \tag{3}$$

The partitioning of the dynamic stiffness matrix into left and right boundaries of the unit cell can be obtained by suppressing the interior degrees of freedom (Mace et al., 2005), hence:

$$\begin{bmatrix} \mathbf{D_{ll}} & \mathbf{D_{lr}} \\ \mathbf{D_{rl}} & \mathbf{D_{rr}} \end{bmatrix} \begin{bmatrix} \mathbf{q_l} \\ \mathbf{q_r} \end{bmatrix} = \begin{bmatrix} \mathbf{F_l} \\ \mathbf{F_r} \end{bmatrix}. \tag{4}$$

The **l** and **r** subscripts are related to the left and right boundaries of the unit cell. Next, let **T** be a matrix that relates displacement and forces between adjacent unit cells. It follows:

$$\begin{bmatrix} \mathbf{q}_\mathrm{l}^{\mathrm{n+1}} \\ \mathbf{F}_\mathrm{l}^{\mathrm{n+1}} \end{bmatrix} = \begin{bmatrix} \mathbf{q}_\mathrm{r}^{\mathrm{n}} \\ -\mathbf{F}_\mathrm{r}^{\mathrm{n}} \end{bmatrix} = \mathbf{T} \begin{bmatrix} \mathbf{q}_\mathrm{l}^{\mathrm{n}} \\ \mathbf{F}_\mathrm{l}^{\mathrm{n}} \end{bmatrix}. \tag{5}$$

Due to Newton's third law, $\mathbf{F_l^{n+1}} = -\mathbf{F_r^n}$. Combining Eqs. (4) and (5), the expression for the transfer matrix **T** is obtained:

$$\mathbf{T} = \begin{bmatrix} -\mathbf{D_{lr}^{-1}}\mathbf{D_{ll}} & \mathbf{D_{lr}^{-1}} \\ -\mathbf{D_{rl}} + \mathbf{D}_{\mathrm{rr}}\mathbf{D_{lr}^{-1}}\mathbf{D_{ll}} & -\mathbf{D_{rr}}\mathbf{D_{lr}^{-1}} \end{bmatrix}. \tag{6}$$

Introducing Floquet-Bloch theorem (Garcia and Fernandez, 2015) in Eq. (5), the eigenvalue problem is stated as:

$$(\mathbf{T} - \lambda\mathbf{I}) \begin{bmatrix} \mathbf{q}_\mathrm{l} \\ \mathbf{F}_\mathrm{l} \end{bmatrix} = 0, \tag{7}$$

where I is the identity matrix and λ the eigenvalues of the transfer matrix. The physical meaning of the eigenvalues is closely connected to the elastic wave propagation of a periodic structure, and it is related to the propagation constant in equation below:

$$\lambda = e^{\mu} = e^{\alpha + j\beta}, \tag{8}$$

where μ is the propagation constant, with its real part α representing the attenuation factor and β the phase constant (Baz, 2019). Thus, if $\alpha = 0$, a pass band condition is defined, as there is no wave amplitude attenuation. If $\alpha \neq 0$, a bandgap

or stop band occurs, as the wave amplitude decays along the periodic structure. Hence, the dispersion diagrams can be plotted using the values of α and β, the attenuation factor diagram and the phase constant diagram respectively.

3. CONFIGURATIONS OF PERIODIC STRUCTURES

In this section it is shown four different configurations of periodic structures that will be used for studying the effects of damping in band gaps and frequency response function. A brief description for each periodic structure is given herein.

Consider the first periodic structure depicted in the left side of Figure 1-A, representing a diatomic phononic crystal (PC). The left side shows the periodic structure composed of masses m_1 and m_2. Each mass is attached by springs k_1 and k_2 and dampers c_1 and c_2. The dashed rectangle bounds the unit cell of this periodic structure, which is displayed on the right side of Figure 1-A. Notice that the mass m_1 is divided in half as it is shown on the right side Figure 1-A.

The second periodic structure is shown in the left side of Figure 1-B, representing a diatomic PC with grounded masses. In this case, the mass m_1 is connected by springs k_1, k_2 and k_3 and dampers c_1, c_2 and c_3, whereas mass m_2 is connected by springs k_1, k_3 and k_4 and dampers c_1, c_2 and c_4. The masses m_1 and m_2 are fixed to the ground, with the former connected to the ground by spring k_2 and damper c_2 and the latter by spring k_4 and damper c_4.The right side of Figure 1-B shows the unit cell configuration. In order to maintain the periodicity, the spring k_2 and damper c_2 is not added to the half mass.

Next, the third configuration of periodic structure is illustrated in the left side of Figure 1-C, representing a monoatomic metamaterial (MM). This configuration is solely composed of mass m_1 in its main chain, and a vibration absorber of mass m_r is added to each mass m_1. The link between m_1 and m_r is achieved by using spring k_r and damper c_r. The connection between the masses of the main chain is obtained by placing spring k_1 and damper c_1. The right side of Figure 1-C shows the unit cell of this periodic structure configuration. Since the mass m_1 was cut in a half, no vibration absorber was added to degree of freedom q_3.

The last periodic structure configuration is pictured in Figure 1-D, and it is similar to the third configuration, with the exception of adding a mass m_2 between masses m_1 in the main chain, representing a diatomic metamaterial. Also, no absorber is connected to the mass m_2. The masses in the main chain are connected via spring k_1 and damper c_1. The vibration absorbers are connected to the masses m_1 through spring k_r and damper c_r. The right side of Figure 1-D shows the unit cell of this periodic structure. Similar to the other cases, the degree of freedom q_4 does not have a vibration absorber attached to it.

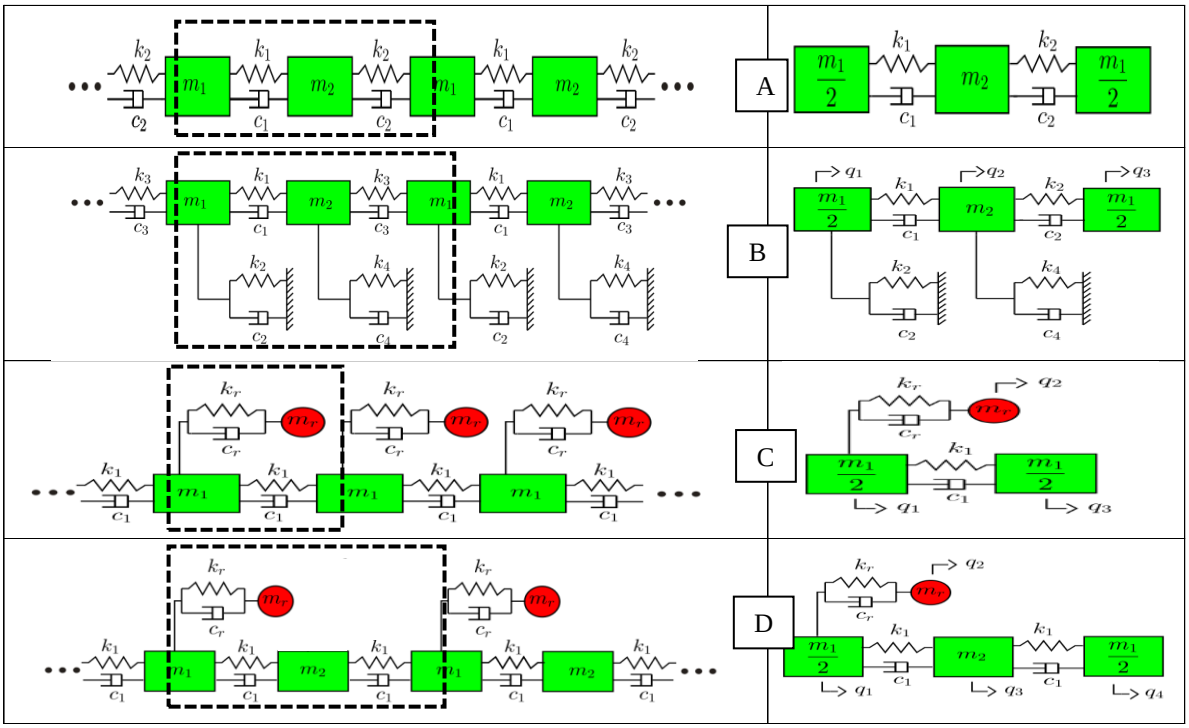

Figure 1. Four configurations along with their unit cells: A-Left Diatomic PC , A-Right Unit cell of diatomic PC, B-Left Diatomic PC with grounded masses, B-Right Unit cell of diatomic PC, C-Left Monoatomic MM, C-Right Unit cell of monoatomic MM, D-Left Diatomic MM, D-Right Unit cell of diatomic MM.

In order to obtain the propagation constant μ to plot the dispersion curves of the periodic structures, the equations of motion for each configuration must be derived so the transfer matrix method can be applied, as discussed in section 2. The equation of motion of the unit cell for the first configuration of periodic cell presented in Figure 1-A is defined in Eq. (9):

$$\begin{aligned} &\tfrac{m1}{2}\ddot{q}_1 + c_1(\dot{q}_1 - \dot{q}_2) + k_1(q_1 - q_2) = f_1, \\ &m_2\ddot{q}_2 + c_1(\dot{q}_2 - \dot{q}_1) + c_2(\dot{q}_2 - \dot{q}_3) + k_1(q_2 - q_1) + k_2(q_2 - q_3) = f_2, \\ &\tfrac{m_1}{2}\ddot{q}_3 + c_2(\dot{q}_3 - \dot{q}_2) + k_2(q_3 - q_2) = f_3. \end{aligned} \tag{9}$$

The set of equations obtained in Eq. (9) are put in matrix form:

$$\mathbf{M}\ddot{\mathbf{q}} + \mathbf{C}\dot{\mathbf{q}} + \mathbf{K}\mathbf{q} = \mathbf{F}, \tag{10}$$

where the mass matrix $\mathbf{M}$, damping matrix $\mathbf{C}$ and stiffness matrix $\mathbf{K}$ are given according to Eq. (9):

$$\mathbf{M} = \begin{bmatrix} \frac{m_1}{2} & 0 & 0 \\ 0 & m_2 & 0 \\ 0 & 0 & \frac{m_1}{2} \end{bmatrix}, \mathbf{C} = \begin{bmatrix} c_1 & -c_1 & 0 \\ -c_1 & c_1 + c_2 & -c_2 \\ 0 & -c_2 & c_2 \end{bmatrix}, \mathbf{K} = \begin{bmatrix} k_1 & -k_1 & 0 \\ -k_1 & k_1 + k_2 & -k_2 \\ 0 & -k_2 & k_2 \end{bmatrix}. \tag{11}$$

The procedure for obtaining mass, stiffness and damping matrices for the other configurations given in Fig.3 - B, C and D, is similar to the process performed for system A. In this case, the mass, damping and stiffness matrices, for the systems B, C and D, are given respectively by Eqs. (12), (13) and (14):

$$\mathbf{M} = \begin{bmatrix} \frac{m_1}{2} & 0 & 0 \\ 0 & m_2 & 0 \\ 0 & 0 & \frac{m_1}{2} \end{bmatrix}, \mathbf{C} = \begin{bmatrix} c_1 + c_2 & -c_2 & 0 \\ -c_2 & c_2 + c_3 + c_4 & -c_4 \\ 0 & -c_4 & c_4 \end{bmatrix}, \mathbf{K} = \begin{bmatrix} k_1 + k_2 & -k_2 & 0 \\ -k_2 & k_2 + k_3 + k_4 & -k_4 \\ 0 & -k_4 & k_4 \end{bmatrix}, \tag{12}$$

$$\mathbf{M} = \begin{bmatrix} \frac{m_1}{2} & 0 & 0 \\ 0 & m_r & 0 \\ 0 & 0 & \frac{m_1}{2} \end{bmatrix}, \mathbf{C} = \begin{bmatrix} c_1 + c_r & -c_r & -c_1 \\ -c_r & c_r & 0 \\ -c_1 & 0 & c_1 \end{bmatrix}, \mathbf{K} = \begin{bmatrix} k_1 + k_r & -k_r & -k_1 \\ -k_r & k_r & 0 \\ -k_1 & 0 & k_1 \end{bmatrix}, \tag{13}$$

$$\mathbf{M} = \begin{bmatrix} \frac{m_1}{2} & 0 & 0 & 0 \\ 0 & m_r & 0 & 0 \\ 0 & 0 & m_2 & 0 \\ 0 & 0 & 0 & \frac{m_1}{2} \end{bmatrix}, \mathbf{C} = \begin{bmatrix} c_1 + c_r & -c_r & -c_1 & 0 \\ -c_r & c_r & 0 & 0 \\ -c_1 & 0 & 2c_1 & -c_1 \\ 0 & 0 & -c_1 & c_1 \end{bmatrix}, \mathbf{K} = \begin{bmatrix} k_1 + k_r & -k_r & -k_1 & 0 \\ -k_r & k_r & 0 & 0 \\ -k_1 & 0 & 2k_1 & -k_1 \\ 0 & 0 & -k_1 & k_1 \end{bmatrix}. \tag{14}$$

4. NUMERICAL RESULTS

In this section the numerical results in terms of dispersion curves and frequency response function (FRF) for the four configurations of phononic crystals and metamaterials are carried out. The damping matrices are modeled as proportional viscous damping, following the classical Rayleigh damping (Chopra, 2017). The damping matrix is given by Eq. (15):

$$\mathbf{C} = a_0\mathbf{M} + a_1\mathbf{K}. \tag{15}$$

Inspecting the damping matrices in Eqs. (11)-(14), it is not possible to obtain a mass proportional damping matrix, as there is no a_0 such that $\mathbf{C} = a_0\mathbf{M}$. Hence, the damping matrices of the four configurations are built using the stiffness proportional term a_1. The expression of the damping ratio of Rayleigh damping (Chopra, 2017) without the mass proportional term is:

$$\zeta_i = \frac{1}{2}a_1\omega_i. \tag{16}$$

The values for the masses and springs in each configuration and prescribed damping ratios are listed in Table 1:

Table 1. List of parameters.

Parameters	Value
m_1, m_2, m_r	$1{,}10{,}10\ [kg]$
k_1, k_2, k_3, k_4, k_r	$100000\ [N/m]$
ζ	$0, 0.005, 0.01, 0.02$

The prescribed damping ratios are applied to the first vibrating mode of each unit cell. The damping coefficients are indirectly obtained from prescribed damping ratio values in Table 1 using Eq. (16).

4.1 Attenuation factor and Phase constant diagram

Now the attention is turned to Figure 2, where the attenuation factor and phase constant diagram of the periodic structures presented in Figure 1 are plotted. The subplots on the left side of Figure 2 show the attenuation factor of each periodic structure for each prescribed damping ratio, whereas the right side of Figure 2 show the phase constant with different damping ratio values. Specifically, Figure 2-a_1) and a_2) shows the attenuation factor and phase constant diagram of the diatomic PC (system A). In Figure 2-b_1) and b_2) it is shown the attenuation and phase constant diagram for the diatomic PC with grounded masses (system B). The monoatomic MM (system C) has its attenuation factor and phase constant diagram depicted in Figure 2-c_1) and c_2). Finally, the dispersion curve showing the attenuation and phase diagrams of the diatomic MM (system D) is shown in Figure 2-d_1) and d_2).

As discussed in Section 2, when the attenuation factor $\alpha \neq 0$, a bandgap condition is defined, therefore it exists an elastic wave amplitude attenuation on a certain frequency range. The phase constant β relates the phase difference between adjacent cells, with its value bounded between 0 and π.

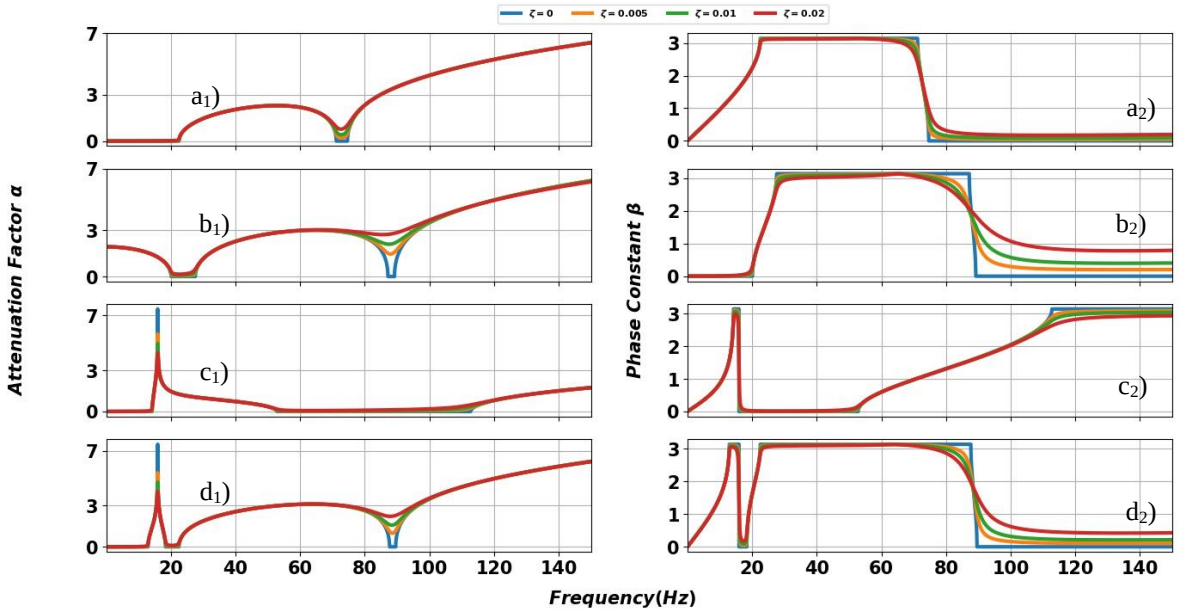

Figure 2. a_1) Attenuation factor diagram of system A, a_2) Phase Constant diagram of system A, b_1) Attenuation factor diagram of system B, b_2) Phase Constant diagram of system B, c_1) Attenuation factor diagram of system C, c_2) Phase constant diagram of system C, d_1) Attenuation factor diagram of system D and d_2) Phase constant diagram of system D.

Starting with the first periodic structure configuration, it is plotted the attenuation factor in Figure 2-a1 and the phase constant in Figure 2-a_1). Regarding the attenuation diagram, it is observed that the pass bands and bandgaps are well defined when no damping is applied. The bandgap regions are observed between the frequency range of 20-75 Hz and between 77 Hz-150 Hz. As the damping ratio increases, the attenuation factor in the pass band region of 75-77 Hz also increases. In this way, it can be stated that a band gap region is created in this frequency interval, leading to a bandgap merging phenomenon. The phase constant of the first periodic structure in Figure 2-a_2) possess the bounding values of zero and pi across the entire frequency range when no damping is applied. However, as damping increases, it is noticeable that such bounding values never occur. This effect is more pronounced at the frequency range of 60 – 150 Hz, and the conclusion drawn from this observation is that when damping is added, the cells will never vibrate in-phase (when phase constant equals zero) or out-of-phase (when the phase constant equals π).

The second configuration shows similar results as in the previous case. In Figure 2-b_1) it is observed three bandgap regions in the attenuation factor diagram corresponding to the frequency range of 0-20 Hz, 27-87 Hz and 90-150 Hz. As the damping ratio increases, especially between the second and third bandgap region, the bandgap merging phenomenon is also observed. The phase constant diagram of Figure 2-b_2) also share similar results with regards to the first periodic configuration. When damping is added to the structure, the bounding values are no more obtainable.

The attenuation factor diagram of the third configuration shown in Figure 2-c_1) presents a local resonance around 16 Hz due to the vibration absorber. It is interesting to notice that the attenuation factor around this resonant frequency diminishes as the damping ratio increases. In this situation thus, it is not advisable to add damping to the vibration absorber if the goal is to decrease the vibration level of the periodic structure. As for the phase constant in Figure 2-c_2), the same conclusion is obtained regarding the bounding values.

Three bandgap regions are displayed for the last configuration, a local resonance type located in the frequency interval of 13-18 Hz and two Bragg types located between 22-87 Hz and 90 -150 Hz take place in the attenuation factor diagram of Figure 2-d_1). The increasing in damping ratio contributes in the lowering of the attenuation factor around the local resonance as in the third configuration, while merging the two bandgaps of Bragg type. The phase constant in Figure 2-d_2) is in agreement with the other three configurations, showing that the bounding values are never achieved with increasing damping ratio values.

4.2 Frequency Response

In order to verify the location of bandgaps and to validate the effect of proportional viscous damping in periodic structures using the dispersion curves of Section 4.1, the frequency response function of the periodic structures studied herein are depicted in Figure 3. In this case, each periodic structure is composed of ten unit cells, and a forced harmonic excitation is applied to the first mass of each periodic structure. The frequency response function of the last mass is then obtained.

The FRF of system A and B are depicted in Figure 3-a) and b), while Figure 3-c) and d) show the FRF of system C and D respectively:

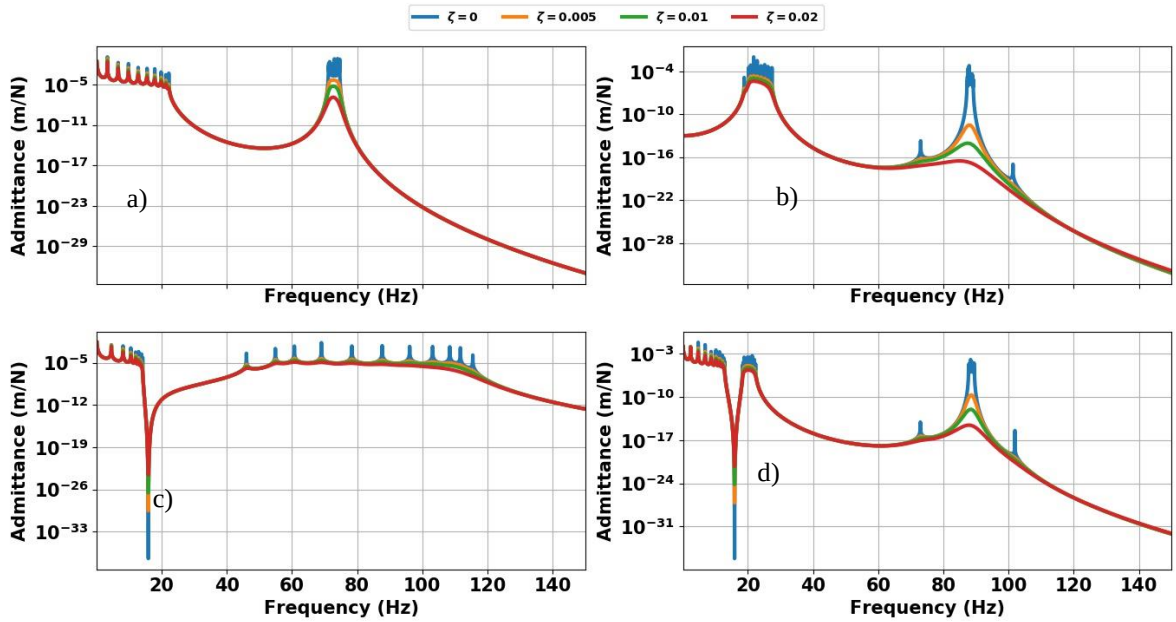

Figure 3. FRF of a) System A PC, b) System B, c) System C and d) System D.

The FRF of the system A in Figure 3-a shows excellent agreement with the attenuation factor diagram of Figure 2-a_1). The two bandgap regions are well defined between the frequency intervals of 20-75 Hz and 77 - 150 Hz. As the damping ratio increases, it is observed that the resonances of the periodic structure are damped. Damping doesn't seem to take effect inside the bandgap regions, as no resonances are found inside of them. Moreover, the bandgap merging phenomenon commented in section 4.1 is seen in the FRF between 75-77 Hz, where the increased damping around this frequency interval leads to lower admittance levels.

As in the previous case, similar results are obtained for the FRF of system B. When the damping ratio increases, the resonant modes are damped, even inside the bandgap regions where two resonances are found in the case of no damping

added. The bandgap merging phenomenon leads to lower admittance levels between 87-90 Hz when the damping ratio is high.

In Figure 3-c) the FRF of system C is plotted. The maximum attenuation factor value located around 16 Hz in Figure 2-c1 matches the lowest admittance level around the same frequency in the FRF chart. Observe that the admittance level increases when raising the damping ratio value. As discussed in section 4.1, the damping in this case contributes to elevate the overall vibration level of the structure when excited at this local resonance frequency, therefore it is not ideal to add damping to the vibration absorber if the objective is to achieve lower vibration levels.

Finally, in Figure 3-d), similar results from system C are obtained in system D. It can be seen that the admittance level of system D increases at 16 Hz when damping is increased, in a similar manner of the third case. It is also observed the bandgap merging phenomenon located between 87 – 90 Hz.

4.3 Spatial Attenuation

In this section, results for the spatial attenuation of the main chain (masses m_1 and m_2) of the periodic systems composed of fifty unit cells are considered. The analysis of the effects of damping is carried out in passbands and bandgaps regions.

In Figure 4 it is shown the spatial attenuation of the four configurations without adding damping. The selected excitation frequency for system A is 72 Hz, and its spatial attenuation is seen in Figure 4 a), whereas systems B, C and D possess an excitation frequency of 88 Hz and have their spatial attenuation illustrated respectively in Figure 4 b), c) and d). According to the attenuation factor diagram of each system in Figure 2 a_1), b_1), c_1) and d_1), these selected excitation frequencies are located in a frequency interval where a passband exists when there is no damping added to the structure.

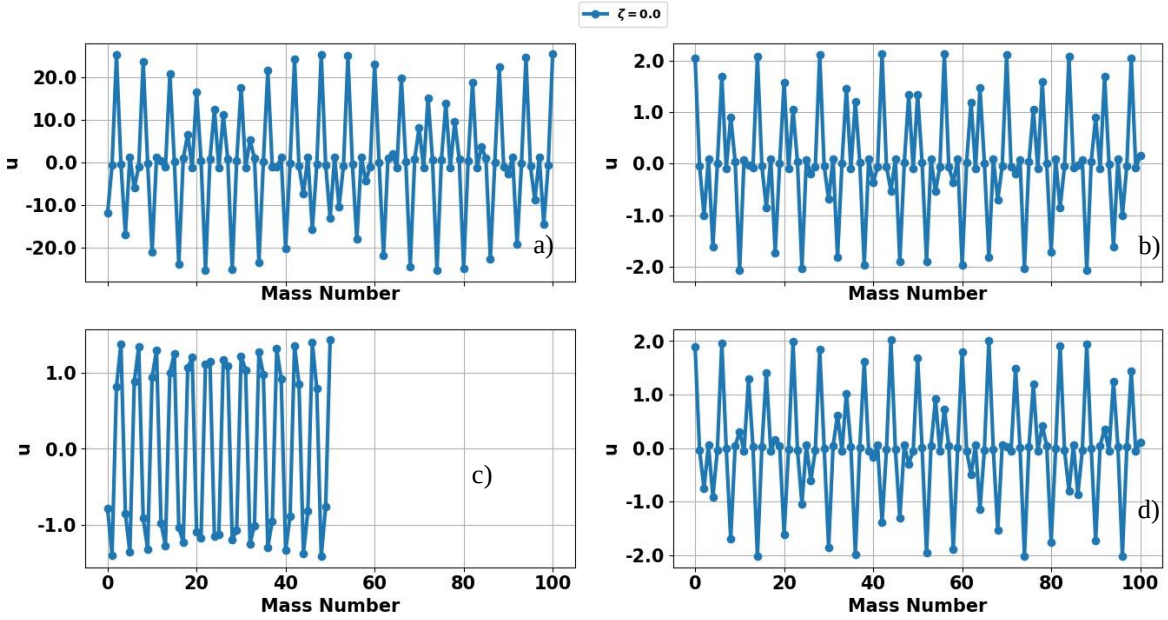

Figure 4. Spatial Attenuation of a) System A with 72 Hz, b) System B with 88 Hz, c) System C with 88 Hz and d) System D with 88Hz, damping is not added.

Since the attenuation factor in these frequencies is zero in a situation where damping is not present, there is no attenuation in the amplitude of the masses across the structure.

Next, in Figure 5, the same excitation frequencies are selected, but this time damping is added to the periodic structures. Figure 5 a), b), c) and d) show the spatial attenuation of systems A, B, C and D respectively when different damping ratios are applied.

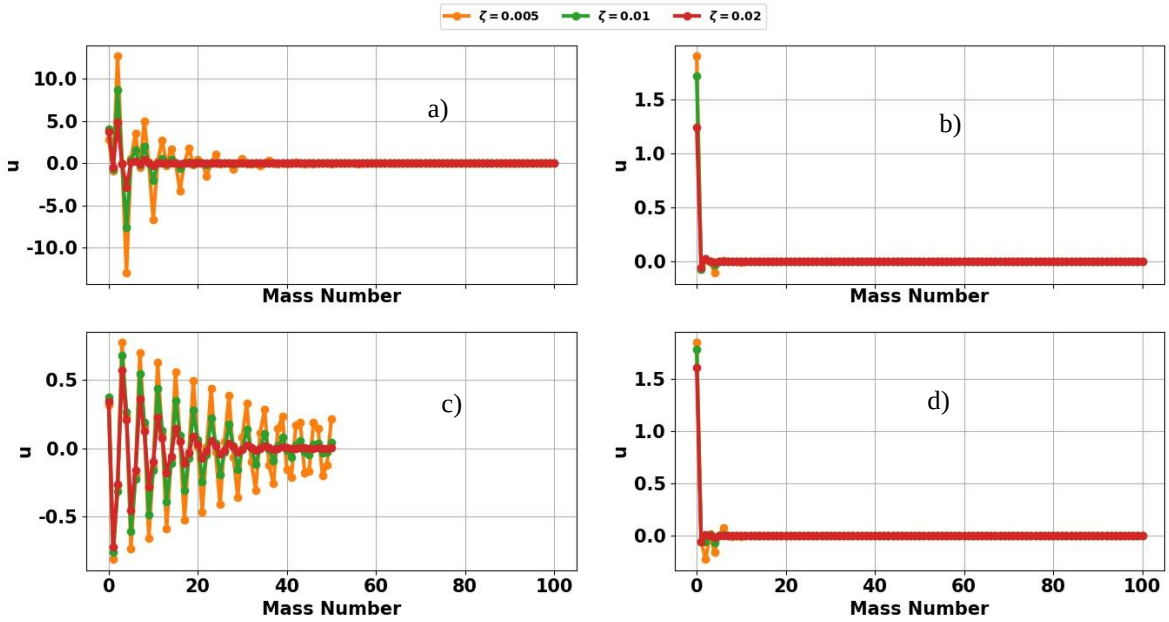

Figure 5. Spatial Attenuation of a) System A with 72 Hz, b) System B with 88 Hz, c) System C with 88 Hz and d) System D with 88Hz, damping is added.

It can be observed from Figure 5 that when damping is present, the movement of the masses are spatially attenuated, regardless of periodic structure configuration. The spatial amplitude attenuation becomes more evident when the damping ratio level is increased. These results corroborate the dispersion diagrams presented in Figure 2, where the passbands become bandgaps when damping is added, and that the attenuation factor level is proportional to the damping ratio level. It is worthy noticing that systems B and D in Figure 5 a) and b) are highly attenuated due to the increased attenuation factor value obtained in their selected excitation frequencies. Moreover, since the system C possess a low attenuation factor value in the frequency range of 88 Hz compared to the other systems as observed in Figure 2 c_1), it is possible to observe the exponential decay in amplitude across the structure.

Results for spatial attenuation in periodic structures without and with proportional damping inside bandgaps are depicted in Figure 6. The excitation frequency is set to 30 Hz, where according to the attenuation factor diagrams in Figure 2, a bandgap region exists when no damping is added. Hence, Figure 6 a), b), c) and d) show the spatial attenuation of systems A, B, C and D respectively inside a bandgap region for various levels of damping ratio.

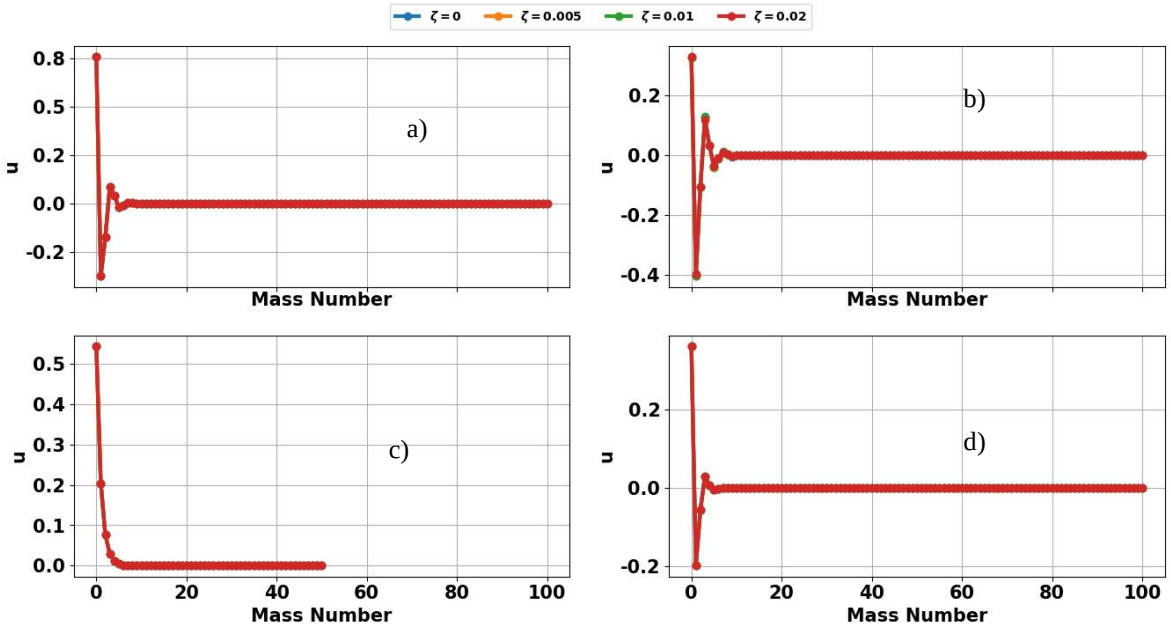

Figure 6. Spatial Attenuation of a) System A, b) System B, c) System C and d) System D at 30 Hz.

It can be seen in Figure 6 that damping takes little effect inside the bandgap regions. The amplitude of the masses is almost the same regardless of damping ratio level. Therefore, it can be concluded that energy dissipation is more pronounced at frequency intervals where bandgaps are not present.

5. CONCLUSIONS

The damping effect in monocoupled phononic crystals and metamaterials were studied in the paper herein. The equation of motion for each unit cell was derived, and the damping was modeled as classical Rayleigh damping. The transfer matrix method was then applied to obtain the attenuation factor and phase constant diagram. It was shown that damping can lead to a bandgap merging phenomenon, where the pass band located between two bandgap regions also transforms into a bandgap. When adding damping to the structure, the phase constant diagrams don't achieve bounding values anymore, in this case the cells of periodic structures will never be fully in or out of phase. Moreover, when damping is added to metamaterials, the attenuation factor value around the local resonance decreases, hence increasing the vibration level at that around that excitation frequency. In order to validate the attenuation factor diagrams, the FRF of each periodic structure configuration was also drawn. Also, spatial attenuation of the four configurations was considered, where it was shown that the effect of damping in the amplitude of the masses is more pronounced in frequency intervals where a passband is present, whereas little effect in spatial attenuation is observed in frequencies where bandgaps exist.

6. ACKNOWLEDGMENTS

The authors acknowledge the financial support provided by the São Paulo Research Foundation (FAPESP), grant #2018=15894-0, Project ENVIBRO) and the Brazilian Research Council (CNPq): D.A. Rade: (grants #310633/2013-3 and #312068/2020-4) and R.A.Borges (grant #439126/2018-5).

7. REFERENCES

Baz, A. M. (2019). *Active and Passive Vibration Damping.* John Wiley & Sons, Ltd.

Beards, C. F. (1996). *Structural vibration : analysis and damping.* London New York: Arnold Halsted Press.

Chopra, A. (2017). *Dynamics of structures : theory and applications to earthquake engineering.* Hoboken, NJ: Pearson.

García, P. G., and Fernández-Álvarez, J.-P. (2015). Floquet-Bloch Theory and Its Application to the Dispersion Curves of Nonperiodic Layered Systems. *Mathematical Problems in Engineering*, *2015*, 1–12.

Hussein, M. I., and Frazier, M. J. (2010, November). Band structure of phononic crystals with general damping. *Journal of Applied Physics*, *108*, 093506.

Hussein, M. I., Leamy, M. J., and Ruzzene, M. (2014). Dynamics of Phononic Materials and Structures: Historical Origins, Recent Progress, and Future Outlook. *Applied Mechanics Reviews*, *66*.

Krattiger, D., Phani, A. S., and Hussein, M. I. (2017). Wave Propagation in Damped Lattice Materials. In *Dynamics of Lattice Materials* (pp. 93–106). John Wiley & Sons, Ltd.

Mace, B. R., Duhamel, D., Brennan, M. J., and Hinke, L. (2005). Finite element prediction of wave motion in structural waveguides. *The Journal of the Acoustical Society of America*, *117*, 2835–2843.